Eigenvalue analysis of size effect for cohesive crack model

YUAN-NENG LI and ZDENĚK P. BAŽANT
McCormick School of Engineering and Applied Science, Northwestern University, Evanston, Illinois 60208, USA

Abstract. The paper analyses the effect of structure size on the nominal strength of the structure that is implied by the cohesive (or fictitious) crack model proposed for concrete by Hillerborg et al. A new method to calculate the maximum load of geometrically similar structures of different sizes without calculating the entire load-deflection curves is presented. The problem is reduced to a matrix eigenvalue problem, in which the structure size for which the maximum load occurs at the given (relative) length of the cohesive crack is obtained as the smallest eigenvalue. Subsequently, the maximum load, nominal strength and load-point displacement are calculated from the matrix equilibrium equation. The nonlinearity of the softening stress-displacement law is handled by iteration. For a linear softening law, the eigenvalue problem is linear and independent of the matrix equilibrium equation, and the peak load can then be obtained without solving the equilibrium equation. The effect of the shape of the softening law is studied, and it is found that the size effect curve is not very sensitive to it. The generalized size effect law proposed earlier by Bažant, which describes a transition between the horizontal and inclined asymptotes of strength theory and linear elastic fracture mechanics, is found to fit the numerical results very well. Finally some implications for the determination of fracture energy from the size effect tests are discussed. The results are of interest for quasibrittle materials such as concrete, rocks, sea ice and modern tough ceramics.

1. Introduction

The basic idea of the cohesive crack model, originated by Barenblatt [1] and Dugdale [2], is that the stress singularity at the crack tip is eliminated by the cohesive (crack bridging) stresses acting across the crack near the crack tip. Various versions exist. In application to metals as well as polymers, the cohesive stresses are assumed to be independent of the deformation near the crack tip. In this study, concerned mainly with quasibrittle materials such as concrete, rocks, tough ceramics and sea ice, we will use the version introduced by Barenblatt [1] and proposed for concrete by Hillerborg et al. [3] (also called the fictitious crack model), in which the cohesive (crack-bridging) stress is assumed to be a function of the crack opening displacement. Because these stresses cannot be considered proportional to the opening displacements, the cohesive crack model is a nonlinear fracture model.

The stress-displacement relation (softening law) of the cohesive crack model approximates the effect of the distributed damage in the fracture process zone and concentrates all the damage into a single line. A counterpart of the cohesive crack model, which is in calculations almost equivalent, is the crack band model (Bažant and Oh [4]) in which the damage in the fracture process zone is assumed to be distributed over a band of certain specified width. Both models are simplifications of reality because the damage is neither concentrated into a line nor distributed over a band of finite width. But such phenomena can be captured only by more complicated models, such as the nonlocal continuum, which are left out of consideration in this paper.

Fracture analysis based on the cohesive crack model is usually carried out by a finite element method. The computational algorithm has been established by [3] and refined by Petersson [5]. Petersson introduced an influence matrix of the nodal displacements along the crack line, condensing the unnecessary degrees of freedom for the other nodes of the structure,

and handled the nonlinearity by iterations. Petersson's method has become standard and has been followed by most subsequent researchers, although with some refinements; for example Carpinteri [6] and Planas and Elices [7].

As it has been recently recognized, the most important practical consequence of fracture mechanics, which distinguishes it from the classical failure theories based on elasticity or plasticity, is the size effect. It is manifested by the dependence of the nominal stress at maximum load (nominal strength) on the structure size of geometrically similar structures. Although the size effect has received considerable attention in recent literature, size effect studies with the cohesive crack model have been scant. Some important results, however, have been obtained by Planas and Elices [8, 7]. Also, Hillerborg presented calculations of broad-range data on the size effect in a three point-bend specimen with a certain stress-displacement law for the cohesive crack, and Bažant [9] showed that these data can be closely approximated by a generalization (Bažant [10]) of the size effect law proposed earlier (Bažant and Oh [4] and Bažant [11]).

The method of calculation of the size effect law in the previous works has been indirect, and required calculation of the entire load-deflection curve. Such calculation is not only unnecessary, but also introduces errors since, due to discretization, none of the calculated points on the curve is likely to be exactly the maximum load point.

The objective of the present paper is to conduct a systematic study of the size effect exhibited by the cohesive crack model and present a new method that allows the maximum loads of geometrically similar specimens of different sizes to be calculated directly, without the rest of the load-deflection curve. Such a direct calculation is made possible by the observation that the response of a monotonically loaded structure with a single mode-I crack that is never closed is path independent and a crack surface potential exists. In the new method, the structure size for a given relative crack length that yields the maximum load is obtained as an eigenvalue of a matrix eigenvalue problem and the condition of singularity of the tangential stiffness matrix can be satisfied exactly. A similar idea has been applied to the cohesive crack model with a linear softening law by Li and Liang [12], Li and Hong [13] and Li and Liang [14]. However, their studies were not aimed at the size effect. Their method applies only to the linear softening law, and cannot be simply generalized to the general nonlinear softening laws.

A secondary objective is to study the effect of the shape of the softening law of the cohesive crack model on the law of the size effect, which has apparently not been thoroughly clarified.

2. Energy principle for structure with cohesive crack

As is shown in Bažant and Cedolin ([15], sec. 10.1, 12.3–12.5), fracture propagation can in general be described on the basis of the potential

$$\mathcal{F} = \Pi + \Psi, \tag{1}$$

understood as the Helmholtz free energy of the structure if the conditions are isothermal. $\Pi = U - W$ = potential energy of the structure; U = strain energy; W = work of loads ($-W$ = their potential energy) and Ψ = surface energy of cracks in the structure. As has been cautioned in [14], crack propagation can be described by a potential only when crack closure is absent or negligible. For linearly elastic structures, we may write

$$U = \frac{1}{2} \int_{\Omega} C_{ijkl} u_{i,j} u_{k,l} \, d\Omega, \qquad W = -P \int_{S_T} b_i u_i \, dS, \tag{2}$$

where a comma before an index denotes a derivative; repeated indices imply summation; Ω = domain occupied by the structure; S_T = boundary on which surface traction Pb_i is applied; b_i = vector field describing the distribution of surface traction over S_T; u_i = displacement vector in Cartesian coordinates x_i,; C_{ijkl} = fourth-rank material stiffness tensor; and P = loading parameter. Finding the maximum value of P is the major concern of this paper.

When the crack growth law is characterized in terms of R-curves, the surface energy $\Psi = \int R(a)da$, where a is the crack length ([15], ch. 12). In the cohesive crack model, there are cohesive forces $\sigma = \varphi(w)$ acting in the process zone in front of the stress-free crack; $w = [u_n]$ is the crack opening, u_n = displacement in the direction n normal to the crack, and [ ] denotes a jump (discontinuity) across the crack. The surface energy is then expressed as ([12])

$$\Psi = \int_{a_0}^a \Phi[w(s, a)]\, ds, \qquad \Phi(w) = \int_0^w \varphi(v)\, dv, \tag{3}$$

where s is the coordinate measured along the crack, $s = a_0$ is the stress-free crack tip, and $s = a$ is the process zone tip.

The first variation of the potential $\mathcal{F}$ yields the equilibrium conditions of the system. The first variation with respect to displacement yields the displacement equilibrium equation

$$\delta_u \mathcal{F} = \int_\Omega C_{ijkl} u_{i,j} \delta u_{k,l}\, d\Omega - P \int_{S_T} b_i \delta u_i\, dS + \int_{a_0}^a \varphi(w) \delta w\, ds = 0, \tag{4}$$

where $\delta w = [\delta u_n]$. This equation is to be satisfied for any admissible displacement variation δu_i. The first variation with respect to crack length a yields the crack equilibrium condition

$$\delta_a \mathcal{F} = \left(\frac{\partial}{\partial a}\Pi + \frac{\partial}{\partial a}\Psi\right)\delta a = 0, \quad \forall \delta a > 0. \tag{5}$$

This equation can equivalently be expressed as $\partial \mathcal{F}/\partial a = (K_\sigma + Pk_P)^2$, in which K_σ is the stress intensity factor at $s = a$ due to cohesive stress in the process zone, and k_P is the stress intensity factor at $s = a$ due to unit applied load, $P = 1$. In other words, the crack equilibrium condition is equivalent to the condition that the total stress intensity factor at $l = a$ is zero, i.e.

$$K_\sigma + Pk_P = 0, \tag{6}$$

which is the basic feature of all cohesive crack models.

To ensure that an adjacent state be also an equilibrium one, it is necessary that $\delta^2 \mathcal{F} = 0$ for variation along the equilibrium path. Separating this second variation into parts corresponding to variation of displacement, crack length and load (labeled by subscripts u, a, and P), we may write this condition as

$$\delta_{uu}\mathcal{F} + \delta_{ua}\mathcal{F} + \delta_{uP}\mathcal{F} = 0,$$
$$\delta_{au}\mathcal{F} + \delta_{aa}\mathcal{F} + \delta_{aP}\mathcal{F} = 0. \tag{7}$$

The second variations of $\mathcal{F}$ can be written more explicitly as

$$\delta_{uu}\mathcal{F} = \int_\Omega C_{ijkl} \delta u_{i,j} \delta v_{k,l}\, d\Omega + \int_{a_0}^a \frac{d\phi}{dw}[\delta u_n][\delta v_n]\, dl \tag{8}$$

and

$$\delta_{uP}\mathcal{F} = \delta P \int_{S_T} b_i \delta u_i \, \mathrm{d}S, \qquad \delta_{aP}\mathcal{F} = \delta P \delta a \frac{\partial}{\partial a} \int_{S_T} b_i u_i \, \mathrm{d}l. \tag{9}$$

Also .

$$\delta_{ua}\mathcal{F} = \delta_{au}\mathcal{F} = \delta a \frac{\partial}{\partial a} \delta_u \mathcal{F}. \tag{10}$$

At the maximum load, the first variation of P must vanish ($\delta P = 0$), and (7) then yields

$$\delta_{uu}\mathcal{F} = \delta a \delta a \frac{\partial^2 \mathcal{F}}{\partial a^2}. \tag{11}$$

Under load control, the maximum load corresponds to the limit of stability (onset of unstable crack propagation). So at P_{max} we must have $\partial^2 \mathcal{F}/\partial a^2 = 0$. This implies that at P_{max} the quadratic form $\delta_{uu}\mathcal{F}$ must be singular, which means that the quadratic form (with $\delta u_i = \delta v_i$) must become zero for some nonzero admissible displacement variation δu_i. This singularity condition is the theoretical basis for the present new method to calculate peak loads without having to calculate the entire load-deflection curves.

3. Problem formulation and finite element approximation

It is convenient to write the given relation of the cohesive (crack-bridging) stress σ to the crack opening w (stress-separation curve) as

$$\sigma = \varphi(w) = f_t[1 - g(w/w_c)], \tag{12}$$

where f_t = direct tensile strength of the material, and w_c = critical crack opening displacement beyond which the cohesive stress is zero. Obviously $g(0) = 0$ and $g(x) = 1$ for $x \geqslant 1$. Since crack closure is prohibited in the process zone, the laws for unloading and reloading need not be specified.

The existence of a unique functional relation between σ and w is the basic hypothesis of the cohesive crack model. Often this hypothesis is not mentioned, however it is certain that in reality there exists no unique relation, for several reasons:

(1) The normal stresses parallel to the crack plane have influence, and so does the loading rate,

(2) w approximates the accumulated damage strain across the width of the fracture process zone, and this width, as well as the damage density in the zone, is variable (depending on structure size and geometry, as well as rate).

Nevertheless, for a certain range of practical applications, a unique relation given by (12) can be assumed to exist as a good approximation, as we do here.

The structure or specimen, which is assumed to be linearly elastic, is discretized by a finite element mesh, as illustrated in Fig. 1 for a three-point-bend fracture specimen which will be considered in numerical computations. The load-point displacement w_1 and the crack opening displacements at the nodes along the crack line (line of symmetry) are grouped into the column matrix $\mathbf{w} = (w_1, w_2, \ldots, w_N)^T$, and the corresponding nodal forces into column matrix $\mathbf{F} = (F_1, F_2, \ldots, F_n)^T$. in which superscript T denotes a transpose. The remaining
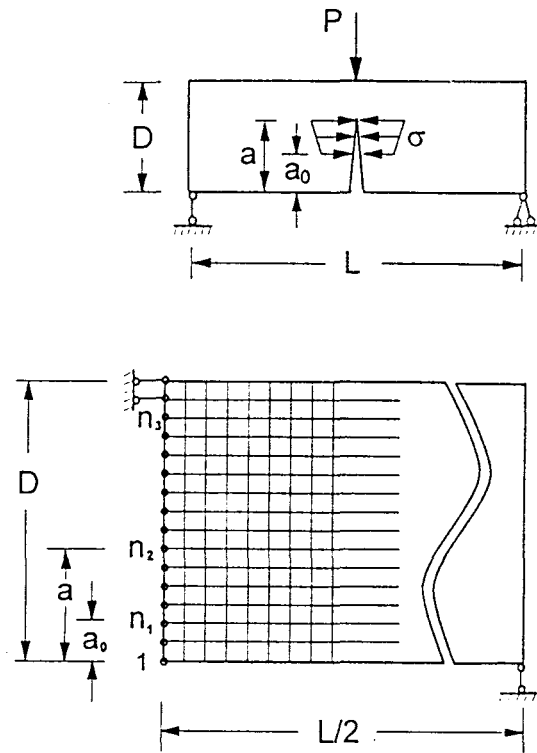
Fig. 1. Geometry dimensions and mesh definition of a three-point bend beam.

nodal displacement and nodal forces for the rest of the structure are grouped into column matrices $\mathbf{w}_R$ and $\mathbf{F}_R$. The associated finite element equation can be written in the partitioned form as

$$\left\{ \begin{array}{c} \mathbf{F} \\ \mathbf{F}_R \end{array} \right\} = - \left[\begin{array}{cc} \mathbf{K}_{CC} & \mathbf{K}_{CR} \\ \mathbf{K}_{RC} & \mathbf{K}_{RR} \end{array} \right] \left\{ \begin{array}{c} \mathbf{w} \\ \mathbf{w}_R \end{array} \right\}. \tag{13}$$

It should be noted that while in the previous section a square bracket is used to denote a jump in the displacement, here it is used to denote a matrix, as it will usually be self-evident in the context. Condensing out all the displacement components of $\mathbf{w}_R$, we obtain the matrix equilibrium equation as $\{\mathbf{F}\} = [\mathbf{K}]\{\mathbf{w}\}$, where $[\mathbf{K}] = [\mathbf{K}_{CC}] - [\mathbf{K}_{CR}][\mathbf{K}_{RR}]^{-1}[\mathbf{K}_{RC}]$ refers only to the load-point displacement and crack-line nodal displacements. It is further convenient to convert this equation to the form

$$\{\mathbf{w}\} = -[\mathbf{C}]\{\mathbf{F}\} + \{\mathbf{B}\}P, \tag{14}$$

where compliance matrices $[\mathbf{C}]$ and $\{\mathbf{B}\}$ have the meaning of crack openings due to unit nodal force on the crack surface and to unit applied load, respectively. Their sizes are $(n \times n)$ and $(1 \times n)$, where $n = N - 1 =$ number of nodes along the crack line.

For the sake of generality, we introduce dimensionless variables as follows

$$\bar{w} = \frac{f_t}{G_f}w, \quad \bar{F} = \frac{F}{bhf_t}, \quad [\bar{\mathbf{C}}] = \frac{E[\mathbf{C}]}{b}, \quad \bar{\sigma}_N = \frac{\sigma_N}{f_t}, \quad \bar{D} = \frac{D}{L_0}. \tag{15}$$

Here $\sigma_N = c_n P/bD =$ nominal stress, $c_n =$ coefficient chosen for convenience such that σ_N would represent the stress at a certain chosen point, for example the maximum stress in a beam

according to the theory of bending; b = thickness of the structure; D = characteristic size (dimension) of the structure (which is in our example chosen to represent the beam depth); h = length of finite elements along the crack, considered to be proportional to D, that is, h/D = constant. Furthermore, we introduce the notation $L_0 = EG_f/f_t^2$ = effective length of the fracture process zone (which is often called the characteristic length, but this term is avoided here because it conflicts with the older definition of the characteristic length of a nonlocal continuum). With these dimensionless variables, we can rewrite (14) as

$$\{\bar{\mathbf{w}}\} = (-[\bar{\mathbf{C}}]\{\bar{\mathbf{F}}\} + \{\bar{\mathbf{B}}\}\bar{\sigma}_N)\bar{D}. \tag{16}$$

In what follows, the bar over the variables will be dropped for the sake of simplicity, with the understanding that all the variables are dimensionless according to (15) unless stated otherwise.

To solve (16) more efficiently, we partition the matrices further. Let $i = 1, 2, \ldots, n_1 - 1$ denote the degrees of freedom on the stress-free crack surface; $i = n_1, n_1+1, n_1+2, \ldots, n_2 - 1$ those in the process zone, and $i = n_2, n_2 + 1, \ldots, n_3$ those in the ligament (Fig. 1). Since the actual crack is closed from the process zone tip and beyond, the corresponding crack opening displacements must be zero. To this end, we divide $\{\mathbf{w}\}$ into two parts: $\{\mathbf{w}_1\}$ includes the displacements along the open crack which includes the stress-free crack and the process zone $(i = 1, 2, \ldots, n_2 - 1)$; $\{\mathbf{w}_2\}$ $(i = n_2, n_2 + 1, \ldots, n_3)$ is zero, by definition. The matrix $[\mathbf{C}]$ and the vectors $\{\mathbf{F}\}$ and $\{\mathbf{B}\}$ are partitioned accordingly. $\{\mathbf{w}_2\}$ is condensed out, so we get

$$\{\mathbf{w}_1\} = (-[\mathbf{C}_{11}^*]\{\mathbf{F}_1\} + \{\mathbf{B}_1^*\}\sigma_N)D, \tag{17}$$

where $[\mathbf{C}_{11}^*] = [\mathbf{C}_{11}] - [\mathbf{C}_{12}][\mathbf{C}_{22}]^{-1}[\mathbf{C}_{21}]$, $\{\mathbf{B}_1^*\} = \{\mathbf{B}_1\} - [\mathbf{C}_{12}][\mathbf{C}_{22}]^{-1}\{\mathbf{B}_2\}$.

In the previous studies, the nodal force has been related to the nodal stress values by assuming that the stress is piecewise constant. However, such an assumption is not sufficiently accurate, especially near the crack tip. In this study, we assume that the stress is linearly distributed from node to node, and so we can write $F_i = (\sigma_{i-1} + 4\sigma_i + \sigma_{i+1})/6$, $i = n_1+1, n_1+2, \ldots, n_2 - 1$. For $i = n_1$, $F_i = (2\sigma_i + \sigma_{i+1})/6$. For $i = 1, 2, \ldots n_1 - 1$, $F_i = 0$. In terms of function $g(w)$, we can write the relation between the nodal forces and nodal stresses as $\{\mathbf{F}_1\} = \{\mathbf{I}\} - [\mathbf{T}_1]\{\mathbf{g(w)}\}$, where $\{\mathbf{I}\}$ is the column matrix that corresponds to the constant part of the stress-separation function $\varphi(w)$ (zero for $i = 1, 2, \ldots n_1 - 1$, 1/2 for $i = n_1$, and 1 for $i = n_1 + 1, n_1 + 2, \ldots, n_2 - 1$), and $[\mathbf{T}_1]$ is a tri-diagonal matrix whose elements are zero whenever one of its indices is within the range 1 and $n_1 - 1$. With these notations, the displacement equilibrium equation becomes

$$\frac{1}{D}\{\mathbf{w}_1\} = \{\mathbf{U}\} - [\mathbf{C}_{11}^*][\mathbf{T}_1]\{\mathbf{g(w)}\} + \{\mathbf{B}_1^*\}\sigma_N, \tag{18}$$

where the column matrix $\{\mathbf{U}\} = [\mathbf{C}_{11}^*]\{\mathbf{I}\}$.

In the ligament, we also assume that the stress distribution is piecewise linear. Therefore, we have similar relations between the nodal forces and the nodal stress values. Such a relation can again be represented symbolically as $\{\mathbf{F}_2\} = [\mathbf{T}_2]\{\sigma_2\}$, where $[\mathbf{T}_2]$ is also a tri-diagonal matrix. Since $\{\mathbf{F}_2\}$ is linearly related to $\{\mathbf{F}_1\}$ and σ_N, the stress at the process zone tip σ_t can be expressed symbolically as

$$\sigma_t = \{\mathbf{S}_1\}^T\{\mathbf{F}_1\} + S_2\sigma_N = 1, \tag{19}$$

which is actually a condition of stress continuity across the process zone tip. The equation for $\{\mathbf{S}_1\}$ and S_2 is straightforward and thus will not be given.
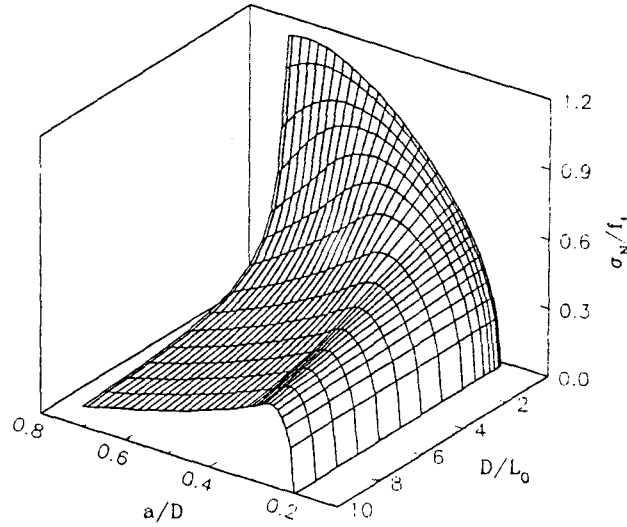
Fig. 2. Nominal strength of structure as a function of size and process zone length.

Equations (18) and (19) are the basic equations of the cohesive crack model and should be solved simultaneously. When the function $g(x)$ is nonlinear, the resulting system of equations is nonlinear, and the iteration method should be employed.

4. Size as an eigenvalue

In Hillerborg's approach, (18) and (19) are solved to obtain the crack opening displacements $\{w_1\}$ and the applied load σ_N for a given size D and given crack length, and the maximum load is then found by searching through different crack lengths. Now we will try to formulate a direct solution approach to obtain the maximum load without having to calculate the entire load deflection curve. The applied load as a function of D and relative crack length a/D is plotted in Fig. 2. It should be emphasized that the maximum is defined only with regard to different a/D. The matrix of the quadratic form $\delta_{uu}\mathcal{F}$ may now be written as

$$\frac{1}{D}[\mathbf{I}] - [\mathbf{C}_{11}^*][\mathbf{T}_1]\left[\frac{d\mathbf{g}}{d\mathbf{w}}\right],\tag{20}$$

where $[\mathbf{I}]$ is the unit matrix, and $[d\mathbf{g}/d\mathbf{w}]$ is a diagonal matrix with nonzero values dg/dw only in the positions corresponding to the nodes in the process zone. The singularity condition is mathematically equivalent to finding a nonzero eigenvector $\{v\}$ such that the following equation be satisfied

$$\frac{1}{D}\{v\}^T = \{v\}^T[\mathbf{C}_{11}^*][\mathbf{T}_1]\left[\frac{d\mathbf{g}}{d\mathbf{w}}\right].\tag{21}$$

For given D (21) can, generally, be satisfied only approximately since a/D can assume only discrete values in accordance to the element mesh. On the other hand, if a/D is given, then (21) can be satisfied exactly because D can vary continuously. In this very sense, (21) becomes a matrix eigenvalue problem, with the largest value of $1/D$ (thus, the smallest D) as the eigenvalue.

For a linear softening law, the matrix $[\mathbf{dg/dw}]$ happens to be a constant matrix. In that case, the eigenvalue problem is linear and independent of the equilibrium solution. Furthermore, by multiplying (18) with the eigenfunction $\{\mathbf{v}\}^T$, one can find for the applied load the equation

$$\sigma_{N^*} = \frac{\{\mathbf{v}\}^T\{\mathbf{U}\}}{\{\mathbf{v}\}^T\{\mathbf{B}_1^*\}}. \tag{22}$$

This value corresponds to the maximum load only when the structure size is equal to the eigenvalue D of (21). The case of linear softening is appealing due to its simplicity.

When the softening is nonlinear, however, such a simple solution is no longer possible. In that case, matrix $[\mathbf{dg/dw}]$ depends on the crack separation $\{\mathbf{w}_1\}$ and the singularity condition is coupled with the equilibrium equation. Iteration must then be used to solve the problem. But the procedure is still straightforward. For a given a/D value, we first solve the linearized eigenvalue problem to obtain an initial guess of D. With the obtained D value, we can solve (18) and (19) to obtain $\{\mathbf{w}_1\}$ as well as the applied load parameter σ_N. Using the value of $\{\mathbf{w}_1\}$ we can then evaluate the tangent matrix $[\mathbf{dg/dw}]$, and obtain a new eigenvalue D. Such a procedure is repeated until the difference between the two succeeding values of D is sufficiently small. The obtained applied load parameter σ_N corresponds to the maximum load when the structure size is the converged value D (in other words, σ_N is not a maximum load if D takes any other value). Next, the value of a/D is changed by a small amount, for instance, a length equal to the element height. The previously solved nodal crack openings are used as the initial estimate to calculate the initial eigenvalue D, and so forth.

This computational strategy is very effective. The actual number of iterations depends on the relative process zone length. Larger relative process zone lengths usually need fewer than 5 iterations to achieve a 4-digit accuracy in D. When the process zone length occupies less than 5 elements, the iteration may fail for some nonlinear softening laws which have extreme slopes (that is, when dg/dw is either very close to zero or very large).

The validity of the solution can be checked using Hillerborg's method. The obtained D is used as the given data, (18) and (19) are solved for different crack lengths. In particular, one may want to check whether the maximum load coincides with the singularity condition. The singularity condition is checked by calculating the determinant of the matrix shown in (20). When the matrix is positive definite, the determinant is positive; when singularity condition is satisfied, the determinant becomes zero. It turns out that, for general nonlinear softening laws, the maximum load occurs at a smaller a/D value than when the determinant becomes zero. Such a discrepancy is obviously caused by the inevitable error introduced by finite element discretization. The basis for this assertion rests on the following facts:

(1) The distance in terms of the relative process zone length between the maximum load and the singularity condition depends on the type of the softening stress-displacement (separation) law. For a linear softening law, there is no discrepancy. For softening laws that are very different from a linear softening law, the distance can be substantial.

(2) The foregoing distance depends also on the relative process zone length. A larger D causes larger discrepancies.

(3) If we use the assumption of piecewise constant distribution of cohesive stress along the crack (which corresponds to replacing the matrices $[\mathbf{T}_1]$ and $[\mathbf{T}_2]$ with unit matrices), the discrepancies are generally much larger. Even for a linear softening law there will be a certain small but appreciable distance between the maximum load and the singularity condition. That is the reason why the assumption of piecewise constant stress distribution causes unnecessary loss of accuracy.
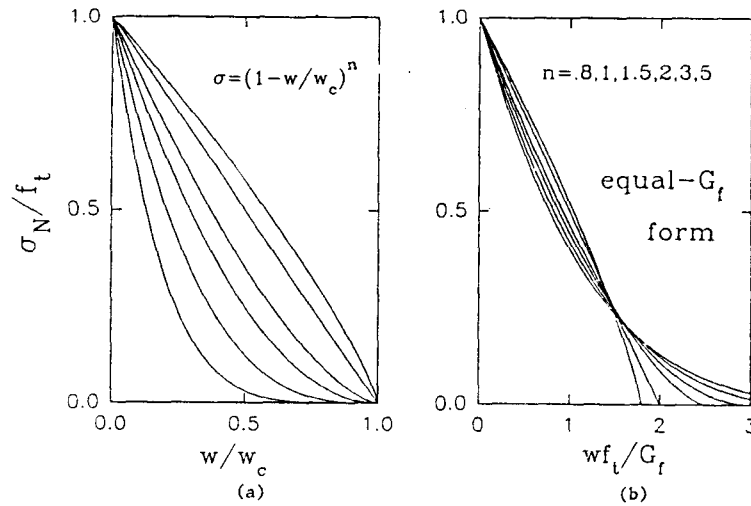
Fig. 3. Power softening curves when normalized by (a) threshold value w_c and (b) G_f/f_t.

5. Numerical results

Calculations have been run for the three-point-bend specimen shown in Fig. 1 having span $L/D = 4$, initial notch-depth ratio $a_0/D = 0.2$ and thickness $b = 1$. The nominal stress is defined as $\sigma_N = 6P/D$, which means that $c_n = 6$. The beam depth is divided into 100 elements. The softening law is considered to be a power function

$$\sigma = \left(1 - \frac{w}{w_c}\right)^n \quad \text{or} \quad \sigma = \left(1 - \frac{\bar{w}}{\bar{w}_c}\right)^n, \quad \bar{w}_c = 1 + n, \tag{23}$$

where n, w_c = given constants; n controls the shape of stress-separation diagram. For different n, the softening curves are plotted in Fig. 3. When plotted against w/w_c, the curves are very different for different n values, as is shown in Fig. 3a. However, when plotted against $\bar{w}$, each curve, by definition, embraces a constant area, and the curves become quite close to each other, although they still substantially differ in the tail portion of the curves because the dimensionless threshold values are very different for different exponents n.

Figure 4 shows, for various values of exponent n, the computed size-effect curves (that is, the curves of dimensionless nominal stress versus dimensionless size $\bar{D} = D/L_0$). The plots are shown in the linear scale on the left and in the log-log scale on the right. This figure reveals an amazing property: the shapes of size-effect curves are not very sensitive to the details of the softening laws. One reason for the proximity of the size-effect curves for various n is that the differences among the different dimensionless softening curves are mostly in the tail portion, which has little effect on the maximum load (although it could be important to the tail of the load-deflection diagram). In the initial portion, the dimensionless softening curves are close to each other and the average slopes are approximately the same.

The proximity of the size effect curves breaks down when the dimensionless softening curves are significantly different in the initial portion. As an example, we compare the linear softening law with the bilinear model for concrete [5], which has its change of shape (knee point) at $\sigma = 0.3f_t$ and $w = 2w_c/9$. Figure 5 shows that the two size effect curves are quite different. For small sizes (say, $\bar{D} < 0.5$), these two curves are parallel in the log-log scale plot. This is because the softening law is in effect linear when only the initial portion of the bilinear
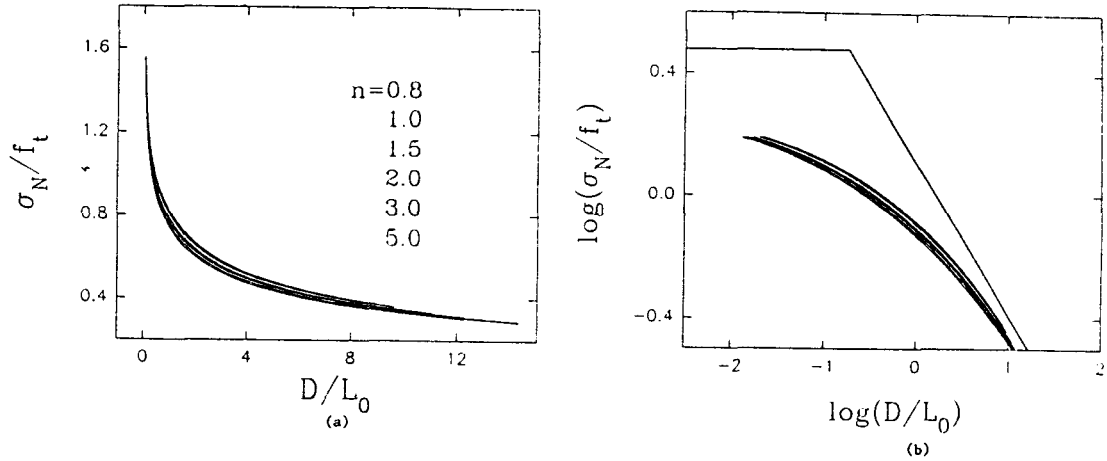
Fig. 4. The size effect curves obtained for power softening in (a) linear coordinate and (b) log-log coordinate.
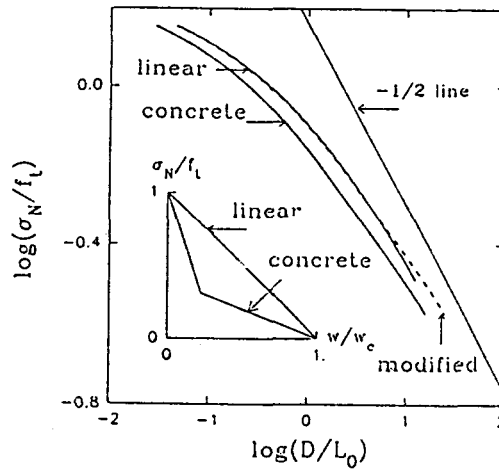

Fig. 5. Size effect curves obtained for linear softening and Petersson's bilinear softening.

softening curve enters the equations. If we shift the curve calculated with the bilinear softening law in the horizontal direction, the two curves can become very close. The dashed line in Fig. 5 is the size effect curve (with a bilinear softening law) that has been shifted by multiplying $\bar{D}$ with 1.58, which is equivalent to redefining $L_0 = EG_f/(1.58f_t^2)$. The difference between the dashed line and the size-effect curve of linear softening becomes significant in the large size range (that is, $\bar{D} > 10$). In other words, it is impossible to deduce an accurate value of material property L_0 from the size effect curve if the size range is not wide enough.

For materials such as concrete which are very heterogeneous on the microscopic scale, the material properties usually exhibit large random scatter. In such cases, the difference between the size effect curves for the linear softening and bilinear softening laws is not important when compared to the random scatter. Therefore, the linear softening model may be preferred in view of its simplicity.

Previous studies of size effect have shown that generally the size effect curve in the plot of log-log scale has two asymptotes. The horizontal one is approached for small sizes, and the inclined one, of slope $-1/2$, is approached for large sizes. A simple formula to describe
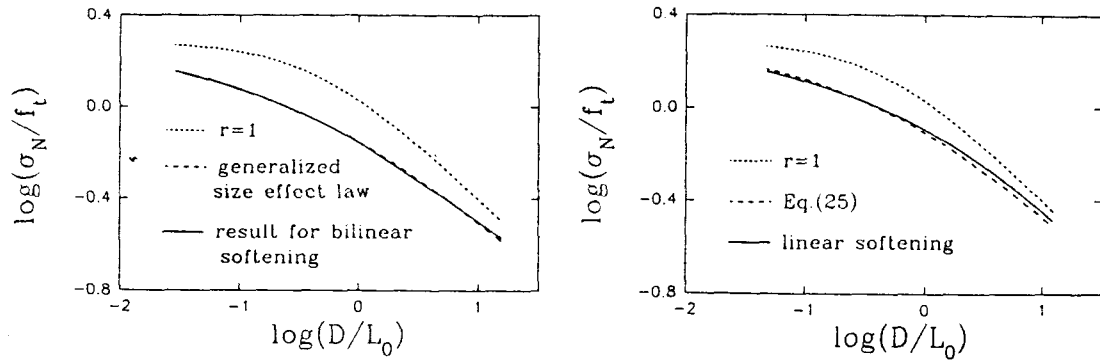
Fig. 6. Size-effect curve calculated by the cohesive crack model and its fit by the generalized form of Bažant's size-effect law.

the size effect curve with these asymptotic properties was derived by Bažant [4, 11], and later generalized to a broad size range in [9, 10]. The stress intensity factor K_e can be calculated at the tip of the process zone caused by the applied load, using the following empirical equation (Tada [16]).

$$\frac{K_e}{\sqrt{EG_f}} = \bar{\sigma}_N \sqrt{D^*} F\left(\frac{a}{D}\right) \quad \text{and}$$

$$F(\xi) = \sqrt{\xi}\frac{1.99 - \xi(1 - \xi)(2.15 - 3.93\xi + 2.7\xi^2)}{(1 + 2\xi)(1 - \xi)^{3/2}}.$$

(24)

For large sizes, the left hand side approaches 1, and thus (24) determines the asymptote of the size effect law for the large size limit. The asymptote in the small size region is a horizontal line $\sigma_N = \beta f_t$. For the three-point-bend specimen with notch ratio 0.2, $\beta = 1.92$ With these two given as asymptotes, Bažant's generalized size effect law can be written as

$$\bar{\sigma}_N = [\beta^{-2r} + (F^2 D^*)^r]^{-1/2r},$$

(25)

where r is the third parameter in addition to parameters L_0 and f_t which are implied in the equation through the dimensionless variables. Figure 6 shows the comparison between (25) and the size effect curves for the cohesive crack model. For the size effect curve obtained with the bilinear (i.e. Petersson's) softening law, the best fit yields $r = 0.4383$; the best fit with the linear softening law yields $r = 0.5092$. Since (25), for both size limits, has the same asymptotic behavior as the cohesive crack model, the proximity between the cohesive crack model solutions and (25) should be considered very satisfactory. In passing we also note that if $r = 1$, the size effect curve, which is also shown in Fig. 6, is very different from the cohesive crack model solutions when a size range of more than 1:20 is considered.

Do the foregoing results mean that the analysis of the test data, determination of G_f and of R-curve, and application in practical design problems such as diagonal shear or torsion should be based on (25) with r approximately equal to 0.5? Not necessarily. Whether the value $r = 0.5$ or $r = 1$ should be used does not really matter for most practical applications to concrete, and it anyway depends on the method chosen for fracture analysis. Although the size effect method for determining G_f or R-curve can be applied for any r value, in most practical applications to concrete the value $r = 1$ may still be appropriate, or at least acceptable. The reason is that the present cohesive crack model cannot be claimed to completely describe the real behavior,
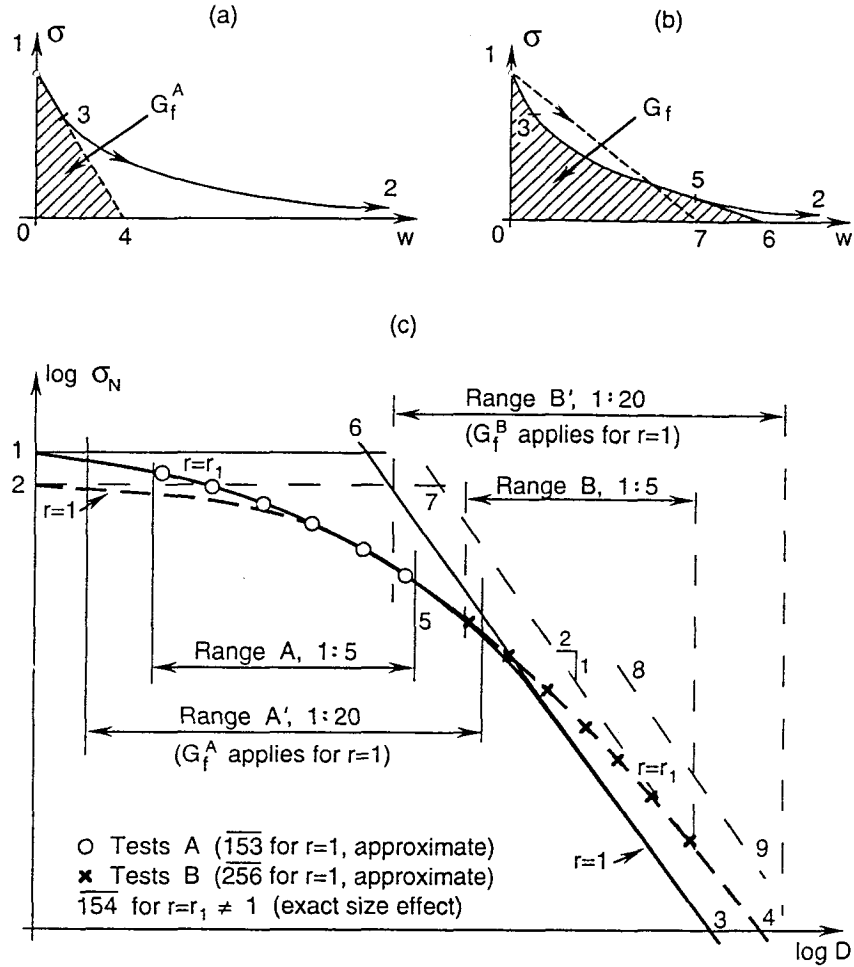
Fig. 7. Size effect curves for narrow and broad size ranges.

because it neglects the rate effect or time dependence, which is very pronounced for concrete, and because it lumps fracturing damage into a line. In reality this damage is spread over a fracture process zone of certain finite width, which likely depends on the structure shape and size as well as the loading rate. The latter aspect can be captured by a nonlocal model for continuum damage, whose optimum approximation could lead to a different r-value from that which we found. Thus, there is at present, no definite general theory that would unquestionably indicate which curve would give the correct representation at all sizes. The existing theories are not experimentally validated beyond a size range of roughly 1:20. So we must inevitably accept that G_f does not correspond to a truly infinite size, but merely to an optimum fit in a size range for which it has been calibrated by tests (or some experimentally verified theory). But this is not a problem from the practical viewpoint, as long as the G_f is used in structural analysis (e.g. in the cohesive crack model or the crack band model) with structure sizes that do not exceed by more than about 1:20 the specimen sizes used for calibration.

Consider now Fig. 7(c) where the given test data A, having the typical limits 1:5, are the circles. Their optimum fit by the size effect law with $r = 1$ is the curve $\overline{123}$, whose asymptote $\overline{63}$ gives (by LEFM calculations) fracture energy G_f^A (as described by Bažant and Pfeiffer,

[17]). When the given test data, having again the range 1:5 are the crosses, fitting the size effect law with $r = 1$ gives the curve $\overline{254}$, whose asymptote $\overline{74}$ gives the fracture energy G_f^B larger than the previous one ($G_f^B > G_f^A$). There may be a certain value $r = r_1$ (for example, $r = 0.5$), applicable to a size range 1:500, for which the size ranges A and B are both fitted well, but there is no theory or experiment to tell us what the r_1 value really is. However the G_f^A value obtained by fitting with $r = 1$ the circular data points will be adequate for the behavior in the size range A'(about 1:20), and the G_f^B value obtained from the crosses will be adequate for the size range B' (1:20). If the size range were extended 100-times beyond the point 4 in Fig. 7, there would likely be still another asymptote $\overline{89}$.

Now, various methods of fracture analysis, such as the R-curve method or the crack band model, are not sufficiently accurate to reproduce the size effect for a range as large as 1:500 with some particular r value. But they agree with the size effect law for $r = 1$ for a limited size range, up to about 1:20. So, if a certain model is calibrated using $r = 1$ by the test data A, G_f^A applies in the size range A' (Fig. 7(c)) but not B'; and if it is calibrated using $r = 1$ by the test data B, G_f^B applies in the size range B' but not A'. This is sufficient for most practical purposes. But one must of course be mindful of the limitations.

As a familiar analogy from the vibration theory, the curve $\overline{154}$ may be compared to the full spectrum, whereas the size effect law for $r = 1$ (curve $\overline{123}$ or $\overline{254}$) may be compared to one spectral component of the spectrum, corresponding to one term in the Fourier expansion of the full spectrum. Or, as another analogy, the curve $\overline{154}$ may be compared to the full compliance function in viscoelasticity, whereas $\overline{123}$ or $\overline{254}$ for $r = 1$ may be compared to one term of its Dirichlet series expansion. As we know, these single components are adequate for representing the behavior in the frequency or delay ranges of about 1:10.

6. Conclusions

1. It is shown that there exists a method which allows direct calculation of the size effect curve for the cohesive crack model without calculating the entire load-deflection curves of specimens of various sizes. Instead of solving, for a given specimen size, the applied load for various crack lengths, the problem can be inverted so that for any chosen relative crack length one seeks directly the structure size for which the chosen relative crack length yields the maximum load. This inverted problem becomes a matrix eigenvalue problem when the structure is discretized by the finite element method, with the structure size as the smallest eigenvalue.

2. After solving the eigenvalue, the displacements and the load can be solved from a matrix equation. This equation, as well as the matrix eigenvalue problem, is nonlinear. Both are coupled if the softening law for the crack-bridging stress is nonlinear, and thus the solution must be iterative. The iteration converges rapidly if the initial estimates of the crack opening displacements are taken as the previously solved displacements for an adjacent crack tip location. Another improvement in the present method compared to the previous finite element solutions is that the stress distribution along the crack line is assumed to vary linearly from node to node, rather than being piecewise constant.

3. The differences in the size effect curves calculated from very different softening laws relating crack-bridging stress to crack opening displacement are not very significant. For power softening laws, very different stress-displacement curves can be obtained by varying the exponent, but the exponent has only a minor effect on the calculated size effect curve.

The difference between the size effect curves for linear softening and for Petersson's bilinear softening law is not negligible. However, when compared with the large scatter inherent to heterogeneous materials such as concrete, the difference seems practically not too important.

4. The calculated size effect curves can be closely matched by the generalized size effect law proposed by Bažant. This means that this law is of rather general applicability. But the preceding conclusion also indicates that one cannot easily deduce the shape of the stress-displacement curve from the shape of the size effect law. One can only deduce the initial slope of this curve.

5. If the cohesive crack model described material behavior over a very broad size range such as 1:1000, it would follow that the determination of the fracture energy G_g from the size effect test should be based on the generalized size effect law with $r \approx 0.5$ rather than $r = 1$. However, the cohesive crack model itself probably is not valid for such a wide range. The value $r = 1$ may still be adequate for a limited size range such as 1:20, provided that the fracture characteristics are calibrated to data lying within that range.

Acknowledgement

References

1. G.I. Barenblatt, *Advances in Applied Mechanics* 7 (1962) 55–129.
2. D.S. Dugdale, *Journal of the Mechanics and Physics of Solids* 8 (1960) 100–104.
3. A. Hillerborg, M. Modéer and P.E. Petersson, *Cement and Concrete Research* 6 (1976) 773–782.
4. Z.P. Bažant and B.H. Oh, *Materials and Structures* (RILEM, Paris) 16 (1983) 155–177.
5. P.E. Petersson, Doctoral dissertation, Lund Institute of Technology, Sweden (1981).
6. A. Carpinteri, in *Application of Fracture Mechanics to Cementitious Composites*, NATO-ARW, S.P. Shah (ed.), Northwestern University (1984) 267–316.
7. J. Planas and M. Elices, *International Journal of Fracture* 51 (1991) 139–157.
8. J. Planas, M. Elices and J. Toribio, in *SEM/RILEN International Conference on Fracture of Concrete and Rock, Recent Developments*, S.P. Shah, S.E. Swartz and B. Barr (eds.), Elsevier Applied Science (1989) 203–212.
9. Z.P. Bažant, in *U.S.-Japan Seminar on Finite Element Analysis of Reinforced Concrete Structures*, Preprints, Tokyo, Vol. 1 (1985) 47–69.
10. Z.P. Bažant, in *Dei Poli Anniversary Volume*, Politecnico di Milano, Italy, L. Cedolin et al. (eds.) (1985) 335–338.
11. Z.P. Bažant, *ASCE Journal of Engineering Mechanics* 110, 4 (1984) 518–535.
12. Y.N. Li and R.Y. Liang, *ASCE Journal of Engineering Mechanics* 118, 3 (1992) 587–603.
13. Y.N. Li and A.P. Hong, *International Journal of Solids and Structures* 29, 23 (1992) 2815–2828.
14. Y.N. Li and R.Y. Liang, *Journal of the Mechanics and Physics of Solids* 41, 2 (1993) 331–350.
15. Z.P. Bažant and L. Cedolin, *Stability of Structures: Elastic, Inelastic, Fracture, and Damage Theories*, Oxford University Press (1991).
16. H. Tada, P.C. Paris and G.R. Irwin, *The Stress Analysis of Cracks Handbook*, Del Research Corporation, Hellertown, PA (1985).
17. Z.P. Bažant and P.A. Pfeiffer, *ACI Materials Journal* 84 (1987) 463–480.